Modelling of the erbium-ytterbium laser

Eric Tanguy, Christian Larat, Jean-Paul Pocholle

Modelling of the erbium–ytterbium laser

E. Tanguy *, C. Larat, J.P. Pocholle

Thomson-CSF, Laboratoire Central de Recherches, Domaine de Corbeville, 91404 Orsay Cedex, France

Abstract

We have developed a modelisation of the Yb:Er glass laser system for pulsed regime. The model is first validated in CW regime with a good agreement with experimental values. The agreement in Q-switch mode is only qualitative. Nevertheless, tendences are outlined due to the particular dynamical behaviour of a codoped system. Especially, we pointed out the possibility of achieving Q-switch operation with pulse repetition frequency greater than the spontaneous de-excitation rate of the erbium upper level without output laser pulse characteristic degradation. On the other hand, gain-switch operation is not well suited for such codoped systems.

1. Introduction

The erbium glass laser is very attractive, mainly due to its emission wavelength located in the 'eye-safe' region [1], in the optical telecommunication window [2], and in a transmission window of the atmosphere. The erbium emission around 1.5 μm has already been demonstrated in the 60s but these lasers operated only at low temperature due to their three-level scheme and the use of lamp pumping [3]. But the energy transfer from ytterbium to erbium ions, the realization of codoped matrices [4], and the room temperature operation of a high power laser diode emitting at 980 nm make the erbium laser very attractive.

The aim of our research is to investigate the dynamical behaviour of such a codoped laser, especially in Q-switched and gain-switched mode. For that reason, we have developed a model which is similar to other ones [5–7], but none of them have investigated these two switched modes.

The model is based on space dependent rate-equation analysis in which the spatial variations of both the pump beam and the laser beam are taken into account. The model is first validated in the CW regime with a good agreement with experimental values. In dynamic resolution, we demonstrate that optimal Q-switch and gain-switch operations are quite difficult to achieve and are very different in this codoped system from a laser singly doped.

2. Theoretical description

In this section we establish the rate equations governing the different level populations and the photon number in the laser cavity.

* Faculté des Sciences et des Techniques de Nantes, Groupe de Physique des Solides pour l'Electronique 2, rue de la Houssinière, BP 92208 Nantes Cedex 03, France. E-mail: tanguy@physique.univ.nantes.fr

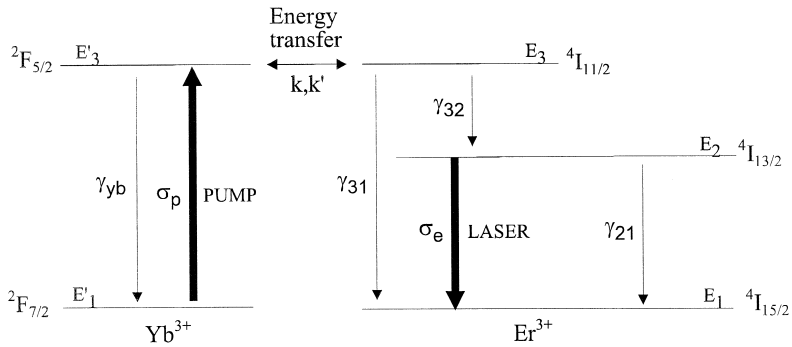

Fig. 1. Simplified energy-level diagram of the erbium–ytterbium system.

2.1. Atomic evolution

The numerical values used in this section are reported in Appendix A.

The pump radiation is absorbed by ytterbium ions (see Fig. 1) which have only two levels. Subsequently, the energy is transferred to the erbium level $^4I_{11/2}$. The back transfer (from erbium to ytterbium) is also possible. The erbium ions which are in the energy level $^4I_{11/2}$ are de-excited to level $^4I_{13/2}$ or $^4I_{15/2}$. The laser transition takes place between the $^4I_{13/2}$ and the fundamental levels. This laser is a three-level one.

For simplification, we assume that the emission cross-section and the absorption cross-section of the laser line are equal. Actually, this fact is true only near the transition peak of the Er ion (1.53 μm). But it is confirmed by our experimental results: the emission wavelength was always near that peak value.

We also neglect any up-conversion (UC) effects for the following reason. It is commonly admitted (see for example Ref. [6]) that the main UC process is due to Er–Er cross relaxation: two Er ions in the metastable state $^4I_{13/2}$ interact leading to one in the ground state $^4I_{15/2}$ and the second in the excited state $^4I_{9/2}$ (above $^4I_{11/2}$). The latter then relaxes in a non-radiative way back to the metastable state $^4I_{15/2}$. Therefore, UC is modelled by a relaxation term quadratic in the concentration of the metastable state (CN_2^2). In our case, $C \cong 10^{-24}$ m^3 s^{-1} (phosphate glasses). Totally excited ions should lead to a UC relaxation rate at least ten times lower than the spontaneous emission rate ($1/\tau_{21}$).

The system is described by the following parameters:

- $N_1(\boldsymbol{r},t)$, $N_2(\boldsymbol{r},t)$ and $N_3(\boldsymbol{r},t)$ (m^{-3}) are respectively the Er^{3+} population densities of the $^4I_{15/2}$ ground state (lower laser level), of the $^4I_{13/2}$ upper laser level and of the $^4I_{11/2}$ level.
- $N_1'(\boldsymbol{r},t)$ and $N_3'(\boldsymbol{r},t)$ (m^{-3}) are respectively the Yb^{3+} population densities of the $^2F_{7/2}$ level and $^2F_{5/2}$ level.
- γ_{ij} (s^{-1}) is the erbium de-excitation rate from the level i to the level j.
- γ_{yb} (s^{-1}) is the de-excitation rate from the Yb^{3+} excited state to the ground state.
- σ_p (m^2) is the Yb^{3+} absorption cross-section at the pump wavelength.
- σ_e (m^2) is the Er^{3+} emission cross-section at the laser wavelength.
- σ_{abs} (m^2) is the Er^{3+} absorption cross-section at the pump wavelength.
- $\Phi_p(\boldsymbol{r},t)$ (m^{-2} s^{-1}) is the pump photon flux.
- $\Phi_l(\boldsymbol{r},t)$ (m^{-2} s^{-1}) is the laser photon flux.
- N_{er} (m^{-3}) is the Er^{3+} atom density.
- N_{yb} (m^{-3}) is the Yb^{3+} atom density.
- k (m^3 s^{-1}) is the energy transfer coefficient from the Yb^{3+} $^2F_{5/2}$ level to the Er^{3+} $^4I_{11/2}$ level.
- k' (m^3 s^{-1}) is the energy transfer coefficient from the Er^{3+} $^4I_{11/2}$ level to the Yb^{3+} $^2F_{5/2}$ level.

On the basis of the level scheme (see Fig. 1), the following space dependent equations for the Er and Yb population densities can be written [8]:

$$\frac{\mathrm{d}N_3'}{\mathrm{d}t} = \sigma_p(N_1' - N_3')\Phi_p - kN_3'N_1 + k'N_1'N_3 - \gamma_{yb}N_3', \tag{1}$$

$$\frac{\mathrm{d}N_3}{\mathrm{d}t} = kN_3'N_1 - k'N_1'N_3 - \gamma_{31}N_3 - \gamma_{32}N_3 + \sigma_{abs}N_1\Phi_p, \tag{2}$$

$$\frac{\mathrm{d}N_2}{\mathrm{d}t} = \gamma_{32}N_3 - \gamma_{21}N_2 - (N_2 - N_1)\sigma_e\Phi_1, \tag{3}$$

$$N_1' + N_3' = N_{yb}, \tag{4}$$

$$N_1 + N_2 + N_3 = N_{er}. \tag{5}$$

This system of equations can be simplified with the following assumptions:

- The Yb^{3+} fundamental level is not depleted by the pump ($N_1' \gg N_3' \Rightarrow N_1' \approx N_{yb}$). A pump power density of about 1 kW/cm^2 is required to obtain $N_3' = 0.01\,N_{yb}$.
- The de-excitation from the Er^{3+} $^4I_{11/2}$ level to the Er^{3+} $^4I_{13/2}$ is more probable than the de-excitation from the Er^{3+} $^4I_{11/2}$ level to the Er^{3+} $^4I_{15/2}$ ($\gamma_{31} \ll \gamma_{32}$). Thus we assume $\gamma_{31} \approx 0$.
- The de-excitation from the Er^{3+} $^4I_{11/2}$ level to the Er^{3+} $^4I_{13/2}$ is fast enough to consider the population in the Er^{3+} $^4I_{11/2}$ level in all cases to be almost stationary (secular approximation: $dN_3/dt \approx 0$) leading to $N_3 = kN_3'N_1/\gamma_{32}$.
- For the same reason, we also neglect the back transfer process from the Er^{3+} $^4I_{11/2}$ level to the Yb^{3+} $^2F_{5/2}$ level ($k'N_1' \ll \gamma_{32}$).
- The pump absorption by the Er^{3+} ground state is also neglected: $kN_3'N_1 \gg \sigma_{abs}N_1\Phi_p$. We can justify that point as follows: in stationary mode $N_3' = \sigma_p N_1'\Phi_p/(kN_1 + \gamma_{yb})$ (from Eq. (6)) leading to the condition: $N_{er}/N_{yb} + \gamma_{yb}/kN_{yb} \ll 1$ $\Rightarrow N_{er}/N_{yb} \ll 1$ and $\gamma_{yb}/kN_{yb} \ll 1$. In our material, the first condition is true because N_{er}/N_{yb} is $\approx 10^{-2}$. The second condition leads to $N_{yb} \gg \gamma_{yb}/k \approx 10^{17}$ cm^{-3} that is also true in our material: N_{yb} is about 10^{21} cm^{-3}.
- $N_2 - N_1 \approx 2N_2 - N_{er}$.

Thus, the atomic evolution is described by the following equations:

$$\frac{dN_3'}{dt} = \sigma_p N_{yb}\Phi_p - kN_3'(N_{er} - N_2) - \gamma_{yb}N_3', \tag{6}$$

$$\frac{dN_2}{dt} = kN_3'(N_{er} - N_2) - \gamma_{21}N_2 - (2N_2 - N_{er})\sigma_e\Phi_1. \tag{7}$$

2.2. Photonic evolution

2.2.1. Beam description

In this section we describe the spatial and temporal properties of the laser beam and the pump beam. We make the following assumptions: (i) the laser oscillates in only one cavity mode, (ii) the cavity is linear, (iii) the laser flux is almost constant in the cavity because gain and losses are small (few percent in our case).

The photon flux Φ is equal to the product of the photon density Ψ in the cavity by the optical wave velocity in the medium:

$$\Phi(\mathbf{r},t) = \frac{c_0}{n}\Psi(\mathbf{r},t), \tag{8}$$

where n is the optical index of the medium and c_0 is the light velocity.

As a consequence of the third assumption, the intracavity intensity is a weak function of z. Thus, the photon number density can be written as

$$\Psi(\mathbf{r},t) = N(t)\varphi(\mathbf{r}), \tag{9}$$

where $N(t)$ is the photon number and $\varphi(\mathbf{r})$ is the spatial density for one photon in the cavity that is defined by

$$\int\int_V\int \varphi(\mathbf{r})dV = 1. \tag{10}$$

Finally, we obtain

$$\Phi(\mathbf{r},t) = \frac{c_0}{n}N(t)\varphi(\mathbf{r}). \tag{11}$$

Expressions of $\varphi(\mathbf{r})$, both for the laser and pump beam, are presented in Appendices B and C respectively.

2.2.2. Equation of evolution

In the laser cavity, the laser photon number variation is the photon number created by stimulated emission minus the loss per unit time. The total photon number created by stimulated emission by time unit in the cavity volume V is

$$\int\int_V\int \sigma_e(N_2 - N_1)\frac{c_0}{n}N_L(t)\varphi_L(\mathbf{r})dV$$

leading to the evolution equation:

$$\frac{\mathrm{d}N_{\mathrm{L}}}{\mathrm{d}t} = -\frac{N_{\mathrm{L}}}{\tau_{\mathrm{cav}}} + \int\int_{V}\int \sigma_{\mathrm{e}}(N_2 - N_1)\frac{c_0}{n}N_{\mathrm{L}}\varphi_{\mathrm{L}}\mathrm{d}V, \tag{12}$$

where N_{L} is the photon number in the cavity. τ_{cav} depends on the cavity losses and the cavity optical length by the relation:

$$\tau_{\mathrm{cav}} = -\frac{2l_{\mathrm{opt}}}{\ln[R(1-p)]c_0}, \tag{13}$$

where l_{opt} is the optical cavity length, R is the output mirror reflection and p is the intrinsic losses per round trip.

It is obvious that if at $t = 0$, $N_{\mathrm{L}} = 0$, Eq. (12) leads to $N_{\mathrm{L}}(t) = 0$ at any time t. Actually, we have neglected the spontaneous emission in the laser mode which do act as a photon injection allowing the induced emission ignition. This phenomenon can be taken into account simply by considering that the initial photon number is non-null (i.e. $N_{\mathrm{L}}(0) = 1$).

2.2.3. Laser output power relation

The output photon number per time unit is $N_{\mathrm{L}}(t)/\tau_{\mathrm{R}}$ where τ_{R} represents the part of τ_{cav} only related to the output mirror transmission: $\tau_{\mathrm{R}} = -2l_{\mathrm{opt}}/\ln(R)c_0$. The output power is thus: $P_1(t) = h\nu_{\mathrm{e}}N_{\mathrm{L}}(t)/\tau_{\mathrm{R}}$ where $h\nu_{\mathrm{e}}$ is the energy of one photon and we obtain the relation:

$$\Phi_1(\boldsymbol{r},t) = \frac{c_0\tau_{\mathrm{R}}}{nh\nu_{\mathrm{e}}}P_1(t)\varphi_1(\boldsymbol{r}). \tag{14}$$

2.3. Global equations

Thus, the laser is described by the three equations:

$$\frac{\mathrm{d}N_3'}{\mathrm{d}t} = \sigma_{\mathrm{p}}N_{\mathrm{yb}}\Phi_{\mathrm{p}} - kN_3'(N_{\mathrm{er}} - N_2) - \gamma_{\mathrm{yb}}N_3', \tag{15}$$

$$\frac{\mathrm{d}N_2}{\mathrm{d}t} = kN_3'(N_{\mathrm{er}} - N_2) - \gamma_{21}N_2 - (2N_2 - N_{\mathrm{er}})\sigma_{\mathrm{e}}\frac{c_0}{n}N_{\mathrm{L}}\varphi_{\mathrm{L}}, \tag{16}$$

$$\frac{\mathrm{d}N_{\mathrm{L}}}{\mathrm{d}t} = -\frac{N_{\mathrm{L}}}{\tau_{\mathrm{cav}}} + \int\int_{V}\int \sigma_{\mathrm{e}}(2N_2 - N_{\mathrm{er}})\frac{c_0}{n}N_{\mathrm{L}}\varphi_{\mathrm{L}}\,\mathrm{d}V. \tag{17}$$

3. Continuous wave analysis

In this section we calculate the continuous wave laser output evolution and compare it with experimental results. All the numerical calculations are performed with Gaussian shape beams except in Section 3.1 where it is compared with the uniform distribution.

3.1. Numerical analysis

In continuous operation, the atomic evolution becomes

$$\text{From Eq. (15):} \quad N_3' = \frac{\sigma_{\mathrm{p}}N_{\mathrm{yb}}\Phi_{\mathrm{p}}}{k(N_{\mathrm{er}} - N_2) + \gamma_{\mathrm{yb}}}, \tag{18}$$

$$kN_3'(N_{\mathrm{er}} - N_2) - \gamma_{21}N_2 - (2N_2 - N_{\mathrm{er}})\sigma_{\mathrm{e}}\frac{c_0}{n}N_{\mathrm{L}}\varphi_{\mathrm{L}} = 0. \tag{19}$$

The resolution of Eqs. (18) and (19) leads to a relation between N_2 and N_{L} as presented in Appendix D.

These equations are numerically solved: we fix the output laser power P_{l} and an arbitrary value of the pump power P_{p} is chosen. Under these conditions, if the calculated gain is greater than the calculated losses, the P_{p} value decreases, and in the other case P_{p} increases. The calculations then converge to the correct pump value. This operation is repeated for different P_{l} values to plot the pump laser versus pump power graph.

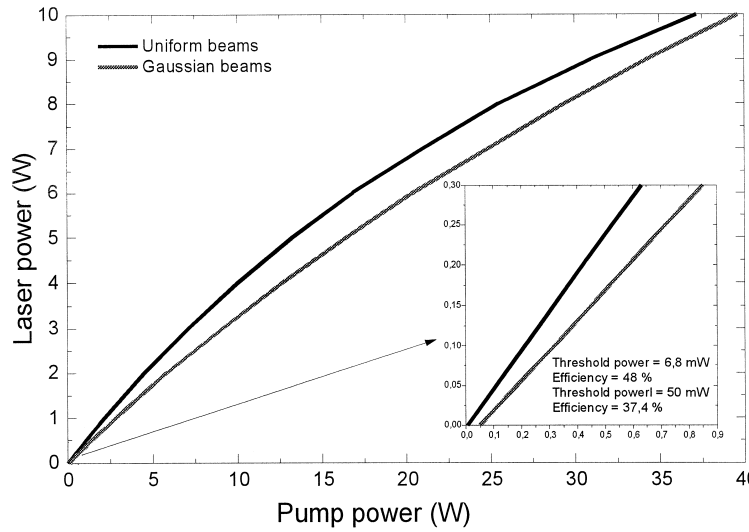

Fig. 2. Laser power versus pump power for uniform and Gaussian beams. No losses – $R = 99\%$ – $w_l = w_p = 100$ μm.

We can verify these equations for certain limit conditions: if we assume that the Yb^{3+} $^2F_{5/2}$ and Er^{3+} $^4I_{13/2}$ have infinite lifetimes ($\gamma_{yb} = 0$ and $\gamma_{21} = 0$), then Eq. (19) leads to: $\sigma_p \Phi_p N_{yb} - (2N_2 - N_{er})\sigma_e (c_0/n) N_L \varphi_L = 0$: one absorbed pump photon creates one laser photon by stimulated emission, because there is no longer atomic relaxation. Considering a uniform spatial distribution for the pump and the laser beam (see Appendices B and C) the threshold power in that case is zero and the efficiency is:

$$\eta = \frac{P_l}{P_p} = \frac{\tau_{cav}}{\tau_R} \frac{\lambda_p}{\lambda_e} (1 - e^{-\alpha l_a}).$$

If there is no other losses than the output mirror loss ($\tau_{cav}/\tau_R = 1$) and if the active material is long enough to absorb all the incident pump power ($e^{-\alpha l_a} = 0$), the laser efficiency is the quantum efficiency: $\eta = \eta_q = \lambda_p/\lambda_e$ as expected.

We can also evaluate the maximum efficiency and the threshold power of the laser with a real material and Gaussian beams (parameters given in Appendix A). In that case, the input/output relation is linear up to 2 W pumping power (see Fig. 2). The 40 W maximum pump power presented in Fig. 2 is actually irrelevant as the assumption of Section 2.1 on the Yb^{3+} depletion failed and as we can expect a fracture of the laser glass at such a high pumping density.

3.2. Numerical versus experimental results

Two different pump sources are investigated: a Ti:Al_2O_3 laser and a pigtailed laser diode. With the first experiment, the intracavity losses (p) and the energy transfer coefficient (k) are adjusted to fit the numerical calculation with the experimental results. These parameter values are then used for the second experiment comparison with no more adjustment.

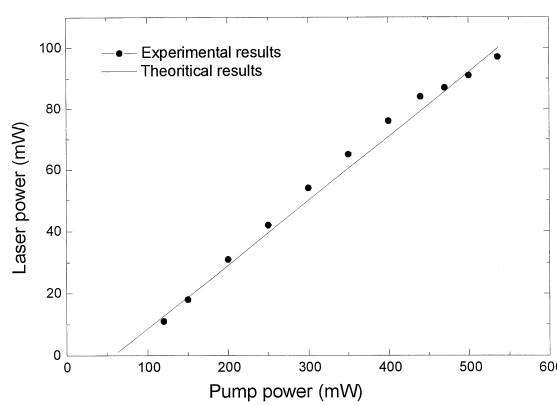

Fig. 3. Laser power versus pump power for experimental and theoretical pumping by a Ti:Al_2O_3 laser.

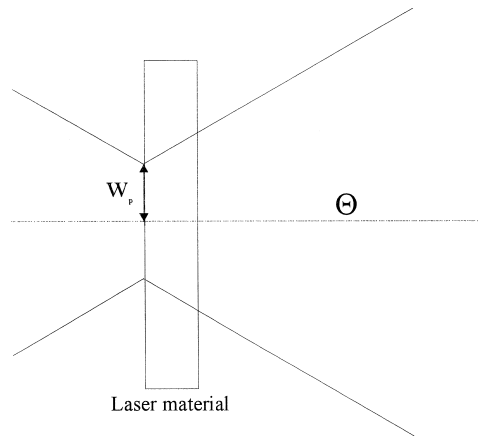

Fig. 4. Pump beam scheme.

3.2.1. Optical pumping by Ti:Al_2O_3 laser

A 2 mm long by a 10 mm diameter Yb:Er:glass disc (Kigre QX/Er) is optically pumped by a Ti:Al_2O_3 laser. One face of the disc is HR coated at 1.54 μm and AR coated at 980 nm. The other face is AR coated at 1.54 μm. The resonator design is a plano–plano cavity with an output mirror of 99%. The Ti:Al_2O_3 laser beam is focused with a 200 mm focal length lens ($w_p = 104$ μm) and is considered to be collimated in the active material (Rayleigh range of 3.5 cm).

The values of the parameters used are presented in Appendix A. We have adjusted k and estimated p (the only parameters not measured) to obtain a good agreement with experimental results. Fig. 3 presents the best fit between experimental and theoretical results. Because of the low gain, this model is very sensitive to the variation of p and k, and we have taken the values of these parameters for which the theoretical results are closest to the experimental results.

3.2.2. Optical pumping by a pigtailed laser diode

With the laser diode pumping the FWHM emission width is greater than that of the absorption transition. So, we have measured the effective absorption and divided it by the Yb^{3+} concentration to obtain an effective absorption cross-section.

The cavity scheme is the same that for Ti:Al_2O_3 pumping except that the end of the fibre (125 μm in core diameter and 0.48 in numerical aperture) is focused in the active material with a magnification of 2.

We have used the same cavity and the same laser material as in the Ti:Al_2O_3 pumping scheme, thus the same parameters have been used, except for the description of the pump beam and for its absorption. The pump beam is described as a Gaussian transverse distribution with a waist w_p and a divergence Θ (see Fig. 4). The parameters used are given in Appendix A. Fig. 5 presents the laser power versus the pump power for experimental and theoretical results. For pump power larger than 500 mW, the experimental curve is not linear. In fact, we have measured the absorption coefficient for all points and it decreases when the pump power increases. The results based on the model are close to the experimental results for pump power less than 500 mW.

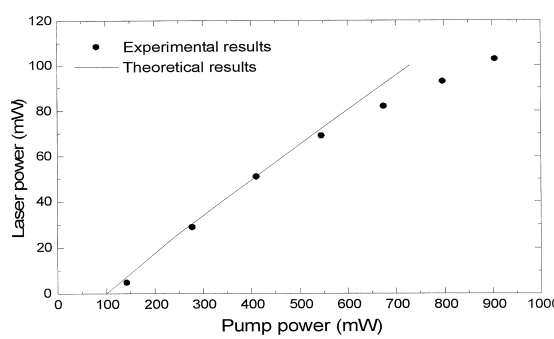

Fig. 5. Laser power versus pump power for experimental and theoretical pumping by a pigtailed laser diode.

4. Dynamic analysis

In this section, we study the dynamical evolution of the laser, both in Q-switch and gain-switch operation.

All the numerical calculations are performed with the uniform distribution (see Appendices B and C). Eq. (12) becomes

$$\frac{\mathrm{d}N_{\mathrm{L}}}{\mathrm{d}t} = N_{\mathrm{L}}\left[-\frac{1}{\tau_{\mathrm{cav}}} + \frac{c_0\sigma_{\mathrm{e}}(2N_2 - N_{\mathrm{er}})}{n_{\mathrm{a}}}\right]. \tag{20}$$

We solve these equations by the Range–Kutta method: with a time increment small enough, we can write: $x(t+\Delta t) = x(t) + (\mathrm{d}/\mathrm{d}t)[x(t)]\Delta t$. The function $x(t)$ can be calculated step by step ($\Delta t = T_{\mathrm{ar}}$ the cavity round trip time).

4.1. Evaluation of the 'energy migration time' from ytterbium to erbium

One interesting parameter for the dynamical behaviour of the laser is the characteristic time (T_{er}) to achieve the metastable state population saturation. We can think about it also as the 'energy migration time' from Yb to Er. An estimation of T_{er} can be made using the following two steps. First we consider the evolution of the upper level of the Yb ions (N_3') without energy transfer to Er ions, leading to an estimation of the N_3' value achievable in the standard case. Secondly, we consider the evolution of the metastable level of the Er ion (N_2) assuming a constant N_3' population value and no laser action.

4.1.1. Ytterbium evolution

Under continuous pumping and $N_{\mathrm{er}} = 0$, the evolution is exponential: $N_3'(t) = N_3'(\infty)[1 - \exp(-t/T_{\mathrm{yb}})]$ with $N_3'(+\infty) = \sigma_{\mathrm{p}}\Phi_{\mathrm{p}}N_{\mathrm{yb}}/(\sigma_{\mathrm{p}}\Phi_{\mathrm{p}} + \gamma_{\mathrm{yb}})$ and the rise time $T_{\mathrm{yb}} = 1/(\sigma_{\mathrm{p}}\Phi_{\mathrm{p}} + \gamma_{\mathrm{yb}})$.

A 1 W pump power on an equivalent area for a Gaussian waist of 100 μm ($\Phi_{\mathrm{p}} = 7\times10^{25}$ m^{-2} s^{-1}) leads to $N_3'(+\infty)/N_{\mathrm{yb}} = 0.088$ and a rise time $T_{\mathrm{yb}} = 920$ μs. We can also point out that the Yb^{3+} ground state population is depleted less than 10%.

4.1.2. Erbium evolution

The $N_2(t)$ evolution with constant N_3' value and without laser action is evaluated. To know the filling time of the Er^{3+} $^4I_{13/2}$ level (N_2), we consider the ytterbium ion (N_3') as a constant energy tank (the level N_3' is not depleted by the energy transfer). In this case Eq. (16) leads to an exponential solution: $N_2(t) = N_2(\infty)[1 - \exp(-t/T_{\mathrm{er}})]$ with $N_2(+\infty) = kN_3'N_{\mathrm{er}}/(kN_3' + \gamma_{21})$ and the rise time $T_{\mathrm{er}} = 1/(kN_3' + \gamma_{21})$.

If $N_3'/N_{\mathrm{yb}} > 10^{-4}$, we find $N_2(+\infty)/N_{\mathrm{er}} > 1/2$ with a rise time $T_{\mathrm{er}} < 4$ ms.

If $N_3'/N_{\mathrm{yb}} > 10^{-3}$ we have $kN_3' \gg \gamma_{21}$, the asymptotical value $N_2(\infty)$ is N_{er} and the rise time T_{er} is $T_{\mathrm{er}} \approx 1/kN_3'$. Due to the strong absorption of ytterbium, such a value for N_3' is easy to achieve ($N_3'(+\infty)/N_{\mathrm{yb}} > 10^{-3} \Rightarrow P_{\mathrm{p}} > 15$ W/cm^2) and thus it is easy to achieve a totally inverted laser transition.

As represented in Fig. 6, the filling time of the Er^{3+} $^4I_{13/2}$ level varies drastically with the population of the Yb^{3+} $^2F_{5/2}$ level. In our case, the asymptotical value (Er^{3+} $^4I_{13/2}$ level population) is always N_{er}. This fact is due to the large ratio between N_{yb} and N_{er} ($N_{\mathrm{yb}}/N_{\mathrm{er}} \approx 100$).

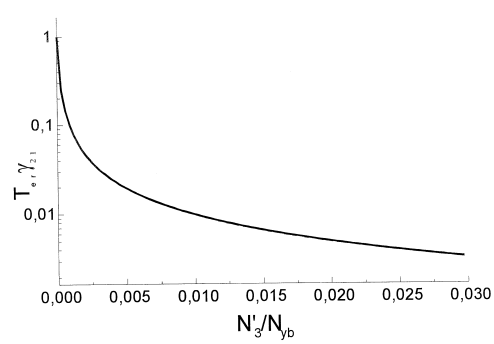

Fig. 6. Population rise time τ_{er} versus population of the Yb^{3+} $^2F_{5/2}$ level.

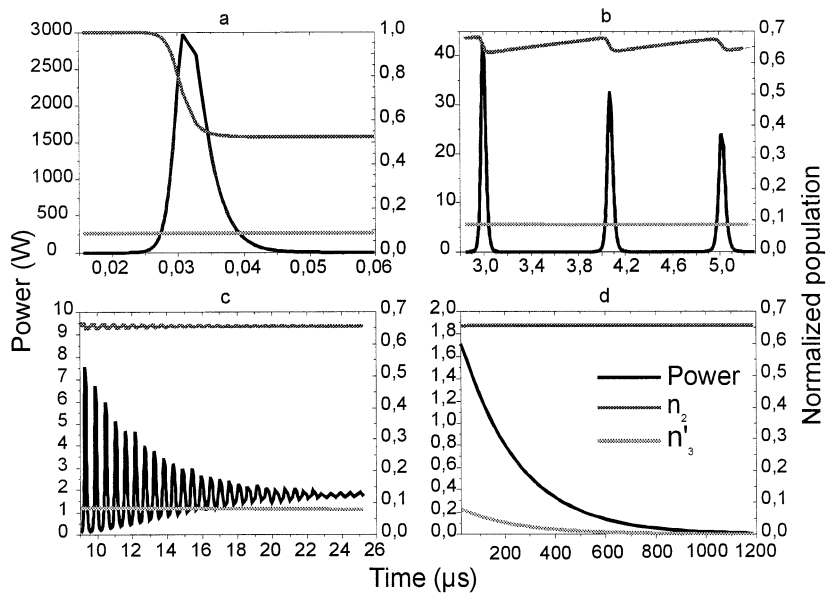

Fig. 7. Temporal evolution of the peak power and population of Yb^{3+} $^2F_{5/2}$ level and Er^{3+} $^4I_{13/2}$ level (time scales are different in the different graphs).

4.2. Q-switch operation

The dynamical behaviour of such a laser in Q-switch operation is investigated. The calculation is performed with uniform distribution for the laser and the pump beams. The material is excited during 8 ms with a 1 W pump power and without laser action (the cavity is blocked). The cavity is instantly switched on and the excitation is turned off.

A first laser pulse is obtained which is typical of classical Q-switched laser operation (Fig. 7a). But energy stored on ytterbium ions excites the erbium ions, again leading to a succession of pulses (Fig. 7b). In fact, this occurs because the pumping of the Er^{3+} ions was not stopped when the pumping of the Yb^{3+} is finished. Due to the large ratio between populations ($N_{yb}/N_{er} \gg 1$), ytterbium acts as a constant pump for erbium [9]. These oscillations corresponds to the classical relaxation oscillation leading to a pseudo free-running mode (Fig. 7c). Finally, as the Yb pumping is, in fact, stopped, the energy tank (N_3') is emptied with a time constant τ ($\tau = [\gamma_{yb} + k(N_{er} - N_2)_{th}]^{-1}$) where $(N_{er} - N_2)_{th}$ is the threshold population of the Er^{3+} ground state. This behaviour was already used to evaluate the energy transfer coefficient [10]. An

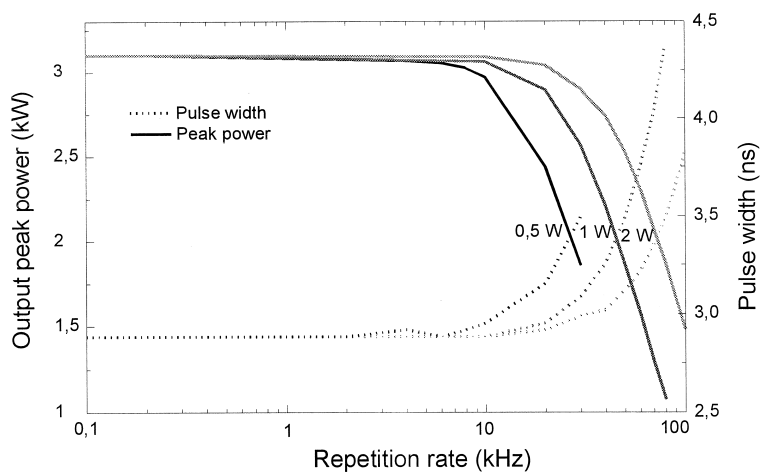

Fig. 8. Output peak power and pulse width versus Q-switch repetition rate.

exponential decrease is obtained for N_3' and P_1 (Fig. 7d) until N_3' is too low to obtain $N_2 = N_2(\text{threshold})$ and the laser stops. After that, N_3' decreases at the rate $(\gamma_{yb} + k(N_{er} - N_2))$, but it is no longer constant as N_2 decreases. The fact that the energy is mainly stored on the ytterbium ions leads to a very poor restitution of this energy in a single laser pulse. So an efficient transfer from the pump energy to the laser pulse needs an optimization of the ratio N_{yb}/N_{er}.

On the other hand, our case is interesting for high pulse repetition frequency Q-switch lasers. Indeed, in continuous pumping we can achieve a pulse repetition frequency much higher than $1/\tau_{21} \approx 100$ Hz with no output laser pulse degradation (see Fig. 8). After the Q-switch pulse, the population N_2 is lower than threshold; N_2 would have to be the same as that before the first pulse to obtain a second Q-switch pulse with the same characteristics. The increase of N_2 is due to the energy transfer from ytterbium to erbium. This transfer decreases the ytterbium population and must be compensated by pumping before the appearance of another Q-switch pulse. Thus the maximum repetition rate is given by the energy transfer rate and the pumping rate and not by the erbium lifetime.

4.3. Gain-switch operation

In the same way, single pulse gain-switch operation is also difficult to achieve because, if the pump is switched off after the laser pulse, the remaining energy stored in Yb^{3+} leads again to other pulses. It is possible to decrease the pump pulse width and/or pump power to obtain a small enough ytterbium population so that, after the energy transfer, the ytterbium upper level population would be small enough to prevent another pulse. This would imply an energy transfer time to obtain population inversion very long (proportional to the ytterbium upper level population) and large output pulse width with low repetition rate would be obtained. So, gain-switch operation is out of interest in that case ($N_{er} \ll N_{yb}$). It could be interesting if $N_{er} \approx N_{yb}$, but in that case, the interest of codoping fails.

4.4. Comparison with experimental results in Q-switch operation

The CW laser presented in Section 3.2.2 has been Q-switched by insertion of a mechanical chopper in the cavity (see Ref. [11] for more details). We have modelled the temporal variation of the intracavity losses due to the chopper as a Gaussian beam cut-off by a disc with slits rotating at a constant frequency:

$$\text{loss} = 1 - \frac{1}{2}\text{erf}\left(\frac{2\sqrt{2}\,\pi rft}{w_1}\right) + \frac{1}{2}\text{erf}\left(\frac{\sqrt{2}\,(2\pi rft - e)}{w_1}\right)$$

with $f = 133$ Hz (rotation frequency), $r = 6$ cm (radius), $e = 500$ μm (slit width) and w_1 the intracavity waist of the laser beam.

The values of the parameters are the same as in Section 3.2.2, with a 1 W pump power. The cavity losses p have been adjusted (the losses introduced by the chopper are not negligible in comparison to the cavity losses). The value $p = 1\%$ corresponds to the best compromise between peak power and pulse width. Nevertheless, the peak power and the pulse width of the first pulse are relatively different (40% and 30%, respectively) and the second pulse is experimentally about 3.3 μs after the first and theoretically about 6.2 μs after the first. In comparison, the experimental output energy is very well fitted by theoretical ones (see Fig. 9). These differences between experimental and theoretical results are probably due to the

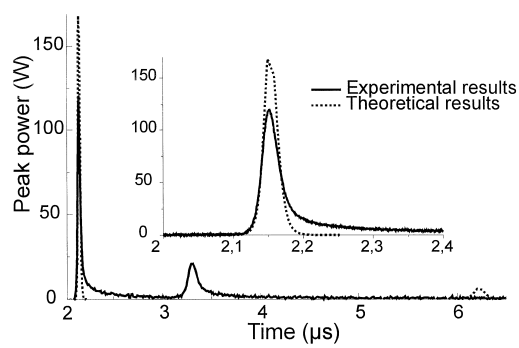

Fig. 9. Temporal profiles of experimental and theoretical pulses.

Table 1

Results	Peak power (W)	Pulse width (ns)	Energy (μJ)
Experimental	120	35	4.2
Theoretical	170	25	4.25

approximation of the temporal variation of the losses and also to the approximation of the beam shape (uniform model). Nevertheless, the order of magnitude of the peak power and the pulse width are good and the model provides a quite accurate estimate of the energy delivered by the laser (Table 1).

5. Conclusion

We have developed a modelisation of the Yb:Er glass laser system. This model is in good agreement with experimental results in steady state, both in Ti:Al_2O_3 pumping and fibre coupled laser diode pumping. The agreement in Q-switch mode is only qualitative. Nevertheless, tendences are outlined due to the particular dynamical behaviour of a codoped system. Especially, we pointed out the possibility of achieving Q-switch operation with pulse repetition frequency greater than the spontaneous de-excitation rate of the erbium upper level without output laser pulse degradation. On the other hand, gain-switch operation is not well suited for such codoped systems.

Appendix A. Parameters used

In this appendix, we give the parameters used for the different simulations.

Common parameters

- Materials:

$\gamma_{21} = 113.6\ s^{-1}$ (measured)
Material index $n = 1.5$
$c_0 = 3 \times 10^8\ m\,s^{-1}$
$\gamma_{yb} = 1000\ s^{-1}$ (measured)
$N_{yb} = 1.6 \times 10^{27}\ m^{-3}$ (measured).
$N_{er} = 1.4 \times 10^{25}\ m^{-3}$ (measured)
$k = 7.1 \times 10^{-21}\ m^3\ s^{-1}$ (adjusted)
$\sigma_e = 7 \times 10^{-25}\ m^2$ (measured)
$\sigma_p = 1.3 \times 10^{-24}\ m^2$ (measured)

- Cavity:

Material length $l_a = 2$ mm
Air length $l_{air} = 2$ mm
$w_p = 10^4$ μm (measured)
$w_l = 88$ μm (measured)
$R = 99\%$
$P = 0.5\%$ (adjusted)

Specific parameters used in Section 3.1
Air length $l_{air} = 0$
$w_p = w_l = 100$ μm
$P = 0$

Specific parameters used in Section 3.2.2 and Section 4.4
$\sigma_p = 6 \times 10^{-25}\ m^2$
$w_p = 110$ μm
$w_l = 80$ μm
$\Theta = 16°$

Appendix B. Laser beam shape

The shape of the laser beam is formalized for the numerical resolution. Two spatial distributions of the laser flux Φ_1 are considered. A uniform one for the sake of simplicity and a Gaussian one more realistic but more TPU consuming. The axis z is in the direction of the propagation and x and y are perpendicular to each other and perpendicular to z.

B.1. Uniform distribution

In this case, we consider a top hat distribution of the laser beam and that the active material fills all the cavity:

$$\varphi_1(\boldsymbol{r}) = \frac{n}{l_{\text{opt}} S},$$

where n is the active material index, l_{opt} is the optical cavity length ($l_{\text{opt}} = n l_{\text{a}}$, l_{a} is the active material length) and S the area of the laser beam.

B.2. Gaussian distribution

In the case of Gaussian shape, we consider that the cavity can be constituted by several materials:

$$\varphi_1(\boldsymbol{r}) = \frac{2n(z)}{l_{\text{opt}} \pi w_1^2} \, \mathrm{e}^{-2r^2/w_1^2},$$

where l_{opt} is the optical cavity length and w_1 the waist of the Gaussian beam. The index of refraction $n(z)$ can vary only along the optical cavity axis.

Appendix C. Pump beam flux shape

The shape of the pump beam flux ($\Phi_{\text{p}}(\boldsymbol{r},t)$) is formalized for the numerical resolution. As for the laser beam description, we consider two cases.

C.1. Uniform distribution

The input pump beam is top hat shaped and matched the laser beam. There is no reflecting surfaces (e.g. output mirror). We assume that the absorbed pump energy is averaged on the whole considered volume.

The photon number absorbed per unit time in the active material is: $[P_{\text{p}}(1 - \mathrm{e}^{-\alpha l_{\text{a}}})]/h\nu_{\text{p}}$ where ν_{p} is the frequency of the pump wave, leading to: $\Phi_{\text{P}} = [P_{\text{p}}(1 - \mathrm{e}^{-\alpha l_{\text{a}}})]/h\nu_{\text{p}} S \alpha l_{\text{a}}$ where S and l_{a} are the same parameters as defined in Appendix B.

C.2. Gaussian distribution

The output face of the laser material presents a non-null reflectivity at the pump wavelength (R_{p}). So we have to consider both the incident pump power and the unabsorbed reflected one.

Let us define $\varphi_0(r,z)$, a one photon spatial density for a pump beam with a lateral Gaussian shape:

$$\varphi_0(r,z) = \frac{2\alpha}{\pi w_{\text{p}}^2 (1 - \mathrm{e}^{-\alpha l_{\text{a}}})} \, \mathrm{e}^{-2r^2/w_{\text{p}}^2} \mathrm{e}^{-\alpha z},$$

where w_{p} is the pump beam waist, α the pump absorption coefficient and l_{a} the active material length. Thus, one can write the pump photon flux as

$$\Phi_{\text{p}}(\boldsymbol{r},t) = \frac{1 - \mathrm{e}^{\alpha l_{\text{a}}}}{\alpha h\nu_{\text{p}}} \left[\varphi_0(r,z) + R_{\text{p}} \mathrm{e}^{-\alpha l_{\text{a}}} \varphi_0(r, l_{\text{a}} - z) \right] P_{\text{p}}(t).$$

Appendix D. Analytical solution

The analytical solution of Eqs. (18) and (19) for the population N_2 is presented,

$$N_2 = \frac{a\gamma_{21} + \gamma_{21}kN_{er} + \gamma_{21}\gamma_{yb} + kaN_{yb} + 2ba + 3bkN_{er} + 2b\gamma_{yb} - \sqrt{\Omega}}{\gamma_{21}k + 2bk},$$

with $a = \sigma_p\Phi_p(\boldsymbol{r},t)$, $b = \sigma_e\Phi_1(\boldsymbol{r},t)$ and

$$\begin{aligned}\Omega = & -2\gamma_{21}k^2aN_{er}N_{yb} + 6\gamma_{21}kN_{er}b\gamma_{yb} + 4b^2kN_{er}\gamma_{yb} + \gamma_{21}^2\gamma_{yb}^2 - 2k^2abN_{yb}N_{er} + 4kabN_{yb}\gamma_{yb} + 4b^2\gamma_{yb}^2 + \gamma_{21}^2a^2 \\ & + 4ka^2N_{yb}b + 2\gamma_{21}\gamma_{yb}kaN_{yb} + 4b^2akN_{er} + 2\gamma_{21}^2akN_{er} + 2\gamma_{21}k^2N_{er}^2b + 2\gamma_{21}^2kN_{er}\gamma_{yb} + 8\gamma_{21}ab\gamma_{yb} + 4b^2a^2 \\ & + \gamma_{21}^2k^2N_{er}^2 + k^2a^2N_{yb}^2 + b^2k^2N_{er}^2 + 4a^2\gamma_{21}b + 2\gamma_{21}^2a\gamma_{yb} + 6\gamma_{21}abkN_{er} + 2a^2\gamma_{21}kN_{yb} + 8b^2a\gamma_{yb} + 4\gamma_{21}\gamma_{yb}^2b.\end{aligned}$$

References

[1] D. Sliney, M. Wolbarsht, Safety with Lasers and Other Optical Sources, Plenum, New York, 1980, p. 145.
[2] I. Joindot, M. Joindot, Les Télécommunications par Fibres Optiques, Dunod, ch. 1, 1996.
[3] Z.J. Kiss, R.C. Duncan, in: J.R. Singer (Ed.), Advances in Quantum Electronics, Columbia University Press, New York, 1961, p. 164.
[4] E. Snitzer, R. Woodcock, Appl. Phys. Lett. 6 (1965) 45.
[5] S. Taccheo et al., Appl. Phys. B 63 (1996) 425.
[6] J. Nilsson et al., IEEE Photonic Technol. Lett. 6 (1994) 383.
[7] P. Laporta, S. Longhi, S. Taccheo, O. Svelto, Optics Comm. 100 (1993) 311.
[8] A.E. Siegman, Lasers, University Science Books, 1986, p. 211.
[9] M. Ding, P.K. Cheo, IEEE Photonic Technol. Lett. 9 (1994) 324.
[10] E. Tanguy, G. Feugnet, J.P. Pocholle, R. Blondeau, M.A. Poisson, J.P. Duchemin, Optics Comm. 145 (1998) 105.
[11] E. Tanguy, J.P. Pocholle, G. Feugnet, C. Larat, M. Schwarz, A. Brun, P. Georges, Electron. Lett. 31 (1995) 458.